eNeuro

Research Article: New Research | Neuronal Excitability

TrkB signaling influences gene expression in cortistatin-expressing interneurons

https://doi.org/10.1523/ENEURO.0310-19.2019

Cite as: eNeuro 2020; 10.1523/ENEURO.0310-19.2019

Received: 1 August 2019
Revised: 14 November 2019
Accepted: 4 December 2019

Manuscript Title Page

1. **Manuscript Title:** TrkB signaling influences gene expression in cortistatin-expressing interneurons

2. **Abbreviated Title:** BDNF-dependent gene expression in Cort neurons

3. **Authors and Affiliations:** Kristen R. Maynard[1*], Alisha Kardian[1*], Julia L. Hill[1] Yishan Mai[1], Brianna Barry[1],Henry L. Hallock[1], Andrew E. Jaffe,[1,2,3,4,5], Keri Martinowich,[1,4,5]

[1]Lieber Institute for Brain Development, Johns Hopkins Medical Campus, Baltimore, Maryland, USA

[2]Department of Mental Health, Johns Hopkins University, Baltimore, MD, USA.

[3]Department of Biostatistics, Johns Hopkins Bloomberg School of Public Health, Baltimore, MD, USA.

[4]Department of Psychiatry & Behavioral Sciences, Johns Hopkins University School of Medicine, Baltimore, MD, USA.

[5]Department of Neuroscience, Johns Hopkins University School of Medicine, Baltimore, MD, USA.

*These authors contributed equally

4. **Author contributions:** KRM, JLH, and KM Designed Research. AK, JLH, YM, BB, KRM and HLH Performed Research. AK, KRM, BB, AEJ Analyzed Data. AK, KRM, AEJ, and KM Wrote the Paper.

5. **Correspondence:**
Keri Martinowich
Lieber Institute for Brain Development
855 North Wolfe Street, Suite 300
Baltimore, MD, 21205.
keri.martinowich@libd.org
(410) 955-1510

6. **Figures:** 4 Main Figures
9 Extended Figures (.CSV, .XLSX, .TIF)

7. **Tables:** 1 Table (Statistical Table)

8. **Multimedia**: No Multimedia

9. **Abstract words**: 163

10. **Significance statement words**: 113

11. **Introduction words**: 706

12. **Discussion words:** 1408

13. **Acknowledgements**: We thank the members of the Lieber Institute RNA Sequencing Core, including Joo Heon Shin, Martha Kimos, and Courtney Williams.

14. **Conflict of Interest**: Authors report no conflict of interest.

15. **Funding Sources:** Funding for these studies was provided by the Lieber Institute for Brain Development, the National Institutes of Mental Health (RO1MH105592 to KM), and the National Institute of General Medical Sciences (T32GM007445 to BKB).

ABSTRACT

Brain-derived neurotrophic factor (BDNF) signals through its cognate receptor tropomyosin kinase B (TrkB) to promote the function of several classes of inhibitory interneurons. We previously reported that loss of BDNF-TrkB signaling in cortistatin-expressing (Cort) interneurons leads to behavioral hyperactivity and spontaneous seizures in mice. We performed bulk RNA sequencing (RNA-seq) from the cortex of mice with disruption of BDNF-TrkB signaling in cortistatin interneurons, and identified differential expression of genes important for excitatory neuron function. Using translating ribosome affinity purification (TRAP) and RNA-seq, we define a molecular profile for Cort-expressing inhibitory neurons and subsequently compared the translatome of normal and TrkB-depleted Cort neurons, revealing alterations in calcium signaling and axon development. Several of the genes enriched in Cort neurons and differentially expressed in TrkB depleted neurons are also implicated in autism and epilepsy. Our findings highlight TrkB-dependent molecular pathways as critical for the maturation of inhibitory interneurons and support the hypothesis that loss of BDNF signaling in Cort interneurons leads to altered excitatory/inhibitory balance.

SIGNIFICANCE STATEMENT

Mounting evidence suggests that brain-derived neurotrophic factor (BDNF) signals through its receptor TrkB to promote inhibitory interneuron function, including a sub-population of cortistatin-expressing (Cort) neurons. This study identifies how TrkB depletion in Cort neurons impacts the Cort interneuron transcriptome as well as gene expression in the surrounding cellular milieu of mouse cortex. Our findings highlight TrkB-dependent molecular pathways in the maturation of inhibitory interneurons and further implicate BDNF signaling as critical for regulating excitatory/inhibitory balance. We identified BDNF-regulation of a number of genes expressed in Cort neurons that are implicated in both autism and epilepsy, which is of note because these conditions are highly comorbid, and are hypothesized to share underlying molecular mechanisms.

INTRODUCTION

Signaling of brain-derived neurotrophic factor (BDNF) via its transmembrane receptor tropomyosin kinase B (TrkB) plays a significant role in the maturation and function of inhibitory neurons in the cortex and hippocampus (Yamada et al., 2002; Alcantara et al., 2006). Although inhibitory GABAergic interneurons represent only 10 to 15 percent of neurons in the rodent cortex (Meyer et al., 2011) they are highly heterogeneous, differing in morphology, firing patterns, response to neuromodulators, and molecular profiles (Tremblay et al., 2016). At least 26 different types of GABAergic interneurons have been identified in the hippocampus (Somogyi et al., 2004), and perhaps more in the cerebral cortex (Myers et al., 2007; Habib et al., 2017). Differences in firing properties, connectivity patterns, and molecular expression profiles are hypothesized to contribute to non-overlapping functions of the respective classes.

BDNF-TrkB signaling plays an important role in the development of several classes of inhibitory interneurons. For example, BDNF regulates the differentiation and morphology of hippocampal interneurons (Marty et al., 1996), and BDNF deletion leads to reduction in several neuropeptide transcripts that define GABAergic populations, including somatostatin (SST), neuropeptide Y (NPY), substance P, and cortistatin (Cort) in the cortex (Glorioso et al., 2006; Martinowich et al., 2011). BDNF decreases the excitability of parvalbumin (Pvalb) interneurons in the dentate gyrus (Nieto-Gonzalez and Jensen, 2013), and accelerates their maturation in the visual cortex (Huang et al., 1999). While BDNF is expressed primarily in excitatory pyramidal neurons, but not in inhibitory interneurons, its receptor TrkB is widely expressed in both excitatory and inhibitory neurons (Cellerino et al., 1996; Gorba and Wahle, 1999; Swanwick et al., 2004). Levels of TrkB expression across different interneuron classes have not been explicitly quantified, but we previously reported that ~50% of Cort-expressing interneurons express TrkB in the cortex (Hill et al., 2019).

Cortistatin is a secreted neuropeptide that is expressed in a distinct set of interneurons. This population partially overlaps with both Pvalb- and SST-expressing inhibitory interneurons, but

its expression is seen prominently in the cerebral cortex and hippocampus (de Lecea et al., 1997). Cortistatin is similar in structure to SST and can bind all fived cloned somatostatin receptors (Veber et al., 1979; Csaba and Dournaud, 2001). However, Cort possesses some notably distinct functions, including its ability to induce sleep slow-wave sleep activity (de Lecea et al., 1996) and regulated synaptic integration by augmenting the hyperpolarization-activated current I_H (Schweitzer et al., 2003). Cortistatin is expressed earlier than most inhibitory neuron markers in the brain, peaking at 2 weeks of age in rodents (de Lecea et al., 1997), which closely parallels the pattern of BDNF expression during neurodevelopment (Katoh-Semba et al., 1997). Reductions in BDNF signaling are associated with decreased expression of *Cort* transcripts (Martinowich et al., 2011; Guilloux et al., 2012), and conversely, administration of cortistatin increases BDNF expression (Souza-Moreira et al., 2013). We previously demonstrated that TrkB expression in Cort interneurons is required to suppress cortical hyperexcitability. Specifically, mice in which TrkB is depleted in Cort interneurons develop spontaneous seizures and die ~1 month after birth. Prior to developing seizures, these mice sleep for significantly less time and display hyperlocomotion (Hill et al., 2019). While this study established that TrkB signaling in Cort interneurons is critical to maintain appropriate levels of cortical excitability, the molecular mechanisms mediating Cort interneuron dysfunction downstream of TrkB signaling remain known.

To better understand the molecular mechanisms by which BDNF-TrkB signaling influences Cort interneuron development and function, we investigated the impact of TrkB deletion in these cells on the Cort interneuron transcriptome as well as gene expression in the surrounding cellular milieu. Translating ribosome affinity purification (TRAP) has been used to identify molecular profiles for many cell types in the mouse brain, including Cort interneurons (Doyle et al., 2008). Here, we used TRAP to assess how TrkB deletion impacts the molecular profile of these cells, and bulk RNA-sequencing (RNA-seq) to assess how this perturbation affects the surrounding milieu. Using this strategy, we identified several differentially regulated genes, including those encoding molecules important for calcium signaling as well as molecules that influence inhibitory/excitatory

160 balance. Identification of the TrkB-dependent gene pathways that support Cort interneuron
161 function contributes to our understanding of cortical hyperexcitability, which is important because
162 changes in cortical excitability have been implicated in several brain disorders, including epilepsy
163 and autism (Wang et al., 2013; van Diessen et al., 2015).
164
165 **MATERIALS AND METHODS**
166 **Animals**
167 We selectively depleted TrkB in Cort-expressing cells by crossing mice in which Cre-
168 recombinase is expressed under control of the endogenous *Cort* promoter, (Cort$^{tm1(cre)Zjh}$/J;
169 referenced in text as Cort^{Cre}, stock# 010910, RRID: IMSR_JAX:010910, Jackson Laboratory, Bar
170 Harbor, ME (Taniguchi et al., 2011)), to mice carrying a *loxP*-flanked TrkB allele (strain fB/fB,
171 referenced in text as TrkB$^{flox/flox}$ (Grishanin et al., 2008; Baydyuk et al., 2011; Hill et al., 2019).
172 Cort^{Cre} mice were received from Jackson Labs on a mixed C57BL/6J × 129S background.
173 TrkB$^{flox/flox}$ mice were maintained on a C57BL/6J background. Cort^{Cre} mice were backcrossed to a
174 C57BL6/J background >12X and TrkB$^{flox/flox}$ mice were backcrossed to a C57BL/6J × 129S
175 background before initiating crosses.
176 For bulk homogenate RNA-seq experiments, the groups were P21 Cort^{Cre} or TrkB$^{flox/flox}$
177 (control group contained both genotypes) and Cort^{Cre}; TrkB$^{flox/flox}$ (experimental group). As seizure
178 onset begins at P21 (Hill et al., 2019), mice may have developed mild seizures by the time of brain
179 extraction. In all RiboTag experiments, the RiboTag mouse (B6N.129-Rpl22$^{tm1.1Psam/J}$; referenced in
180 text as Rpl22^{HA}, stock #011029, RRID: IMSR_JAX:011029, Jackson Labs (Sanz et al., 2009)) was
181 used, which expresses a hemagglutinin (HA) tag on the ribosomal protein RPL22 (RPL22^{HA}) under
182 control of Cre-recombinase. For RiboTag experiments in Cort neurons, the groups were adult
183 Cort^{Cre}; Rpl22^{HA} Input vs. Cort^{Cre}; Rpl22^{HA} Immunoprecipitation (IP). For RiboTag experiments in
184 TrkB-deleted vs TrkB-intact Cort neurons, the groups were P21 Cort^{Cre}; Rpl22^{HA} mice and Cort^{Cre};
185 TrkB$^{flox/flox}$; Rpl22^{HA} mice (experimental group).

All mice were housed in a temperature-controlled environment with a 12:12 light/dark cycle and *ad libitum* access to standard laboratory chow and water. Mice were group housed based on genotype. All experimental animal procedures were approved by the SoBran Biosciences Institutional Animal Care and Use Committee. Male and female mice were included and analyzed for all experiments.

RNA extraction and qPCR

Mice were cervically dislocated and cortices were flash frozen in isopentane. For bulk homogenate experiments in P21 control and $Cort^{Cre}$;$TrkB^{flox/flox}$ mice, RNA was extracted using TRIzol (Life Technologies, Carlsbad, CA), purified using RNeasy minicolumns (Qiagen, Valencia, CA), and quantified using a Nanodrop spectrophotometer (Agilent Technologies, Savages, MD). RNA concentrations were normalized and reversed transcribed using Superscript III (Life Technologies). Quantitative PCR (qPCR) was performed using a Realplex thermocycler (Eppendorf, Hamburg, Germany) with GEMM mastermix (Life Technologies) and 40 ng of synthesized cDNA. Individual mRNA levels were normalized for each well to *Gapdh* mRNA levels. For validation of genes differentially expressed in control and experimental Ribotag samples, cDNA was synthesized using the Ovation RNA Amplification System V2 kit (described below) and qPCR was performed as above. Taqman probes were commercially available from Life Technologies (Gad1 Mm00725661_s1, Cort Mm00432631_m1, Gfap Mm01253033_m1, Wt1 Mm01337048_m1; Cxcr4 Mm01292123_m1; Calb1 Mm00486647_m1; Lgals1 Mm00839408_g1; Trpc6 Mm01176083_m1; Syt6 Mm04932997_m1; Gng4 Mm00772342_m1; Ttc9b Mm01176446_m1; S100a10 Mm00501458_g1; Nxph1 Mm01165166_m1; Syt2 Mm00436864_m1; Gsn Mm00456679_m1) or as described in (Martinowich et al., 2011) . Statistical analysis was conducted using GraphPad Prism Software (La Jolla, CA). Comparisons between two groups were performed using unpaired Student's t-test. Data are presented as mean ± SEM and statistical significance was set at *P <0.05, **P <0.01, ***P<0.001, ****P<0.0001.

RNAscope single molecule fluorescent in situ hybridization (smFISH)

Control and Cort^{Cre};TrkB$^{flox/flox}$ P21 mice were cervically dislocated and the brains were removed from the skull, flash frozen in isopentane, and stored at −80°C. Brain tissue was equilibrated to −20°C in a cryostat (Leica, Wetzlar, Germany), and serial sections of cortex were collected at 16 µm. Sections were stored at −80°C until completion of the RNAScope assay. We performed smFISH utilizing the RNAscope Fluorescent Multiplex Kit v2 (Cat # 323100 Advanced Cell Diagnostics [ACD], Hayward, California) according to (Colliva et al., 2018) . Briefly, tissue sections were fixed with a 10% neutral buffered formalin solution (Cat # HT501128 Sigma-Aldrich, St. Louis, Missouri) for 20 min at room temperature and pretreated with protease IV for 20 min. Sections were incubated with commercially available *Wt1* (Cat # 432711, ACD) and *Cre* (Cat # 312281-C2, ACD) probes. Probes were fluorescently labeled with orange (excitation 550 nm), green (excitation 488 nm), or far red (excitation 647) fluorophores using the Amp 4 Alt B-FL. Confocal images were acquired in z-series at 63x magnification using a Zeiss 700LSM confocal microscope. Images were blinded, and transcript co-localization was quantified using custom MATLAB functions. Briefly, cell nuclei were isolated from the DAPI channel using the cellsegm toolbox (gaussian smoothening, adaptive thresholding and splitting of oversized segmented nuclei) (Hodneland et al., 2013). Once centers and boundaries of individual cells were isolated, an intensity threshold was set for transcript detection, and watershed segmentation was used to split detected pixel clusters in each channel into identified transcripts. Custom MATLAB functions were then used to determine the size of each detected transcript (regionprops3 function in Image Processing toolbox). Each transcript was then assigned to a nucleus based on its position in 3 dimensions. Transcripts with centers outside the boundaries of a nucleus were excluded from further analysis. A cell was considered to be positive for a gene if more than 2 transcripts were present.

Bulk cortex RNA-seq

Cortices of control (n=5) and Cort^{Cre}; TrkB$^{flox/flox}$ (n=5) mice were collected and flash frozen in isopentane. RNA was extracted from one hemisphere of each animal using TRIzol (Life Technologies, Carlsbad, CA), purified with RNeasy minicolumns (Qiagen, Valencia, CA), and

quantified using Nanodrop. The Nextera XT DNA Library Preparation Kit was used to generate sequencing libraries according to manufacturer instructions. Samples were sequenced on the HiSeq2000 (Illumina).

Ribotag and RNA-seq of Cort interneurons

Cortices of $Cort^{Cre}$; $Rpl22^{HA}$ mice (n=3) were collected and flash frozen in isopentane. For each sample (n = 3 Input and n = 3 IP), one hemisphere of the cortex from each animal was homogenized according to previously described protocols (Sanz et al., 2013). An aliquot of homogenate was flash frozen and reserved for "Input" samples. Ribosome-mRNA complexes ("IP" samples) were affinity purified using a mouse monoclonal HA antibody (MMS-101R, RRID: AB_2565334, Covance, Princeton, NJ) and A/G magnetic beads (88803 Pierce). RNA from Input and IP samples was purified using RNeasy microcolumns (Qiagen, Valencia, CA) and quantified using the Ribogreen RNA assay kit (R11490 Invitrogen). Sequencing libraries were prepared using the SMARTer Stranded RNA-Seq kit (Clonetech) and sequenced on the HiSeq2000 (Illumina).

Ribotag and RNA-seq of Cort interneurons following disruption of BDNF-TrkB signaling

Cortices of control (n=6) or $Cort^{Cre}$; $TrkB^{flox/flox}$; $Rpl22^{HA}$ (n=6) mice were collected and flash frozen in isopentane. One hemisphere of the cortex from each animal was homogenized according to previously described protocols (Sanz et al., 2013). Sixty-five microliters of total homogenate was flash frozen and reserved for "Input" samples. Ribosome-mRNA complexes ('IP' samples) were affinity purified using a mouse monoclonal HA antibody (MMS-101R, Covance, Princeton, NJ) and A/G magnetic beads (88803 Pierce). RNA from Input and IP samples was purified using RNeasy microcolumns (Qiagen, Valencia, CA) and quantified using the Ribogreen RNA assay kit (R11490 Invitrogen). The Ovation RNA Amplification System V2 kit (7102 Nugen, San Carlos, CA) was used to amplify cDNA from 10 ng of RNA according to manufacturer's instructions. cDNA was used for qPCR validation for *Cort* enrichment in IP versus Input samples. Sequencing libraries were generated with the Ovation SoLo RNA-seq System Mouse (0502–32 Nugen, San Carlos, CA)

according to manufacturer's instructions from 10 ng of RNA. Library concentration was quantified using the KAPA Library Quantification Kit (KR0405, KAPA Biosystems, Wilmington, MA). Libraries were sequenced using the MiSeq Reagent Kit v3 (MS-102–3001 Illumina, San Diego, CA) and Nugen Custom SoLo primer.

RNA-seq data processing and analyses

RNA-seq reads from all experiments were aligned and quantified using a common processing pipeline. Reads were aligned to the mm10 genome using the HISAT2 splice-aware aligner (Kim et al., 2015) and alignments overlapping genes were counted using featureCounts version 1.5.0-p3 (Liao et al., 2014) relative to Gencode version M11 (118,925 transcripts across 48,709 genes, March 2016). Differential expression analyses were performed on gene counts using the voom approach (Law et al., 2014) in the limma R/Bioconductor package (Ritchie et al., 2015) using weighted trimmed means normalization (TMM) factors using the statistical models described below. For each analysis, multiple testing correction was performed using the Benjamini-Hochberg approach to control for the false discovery rate (FDR; (Kasen et al., 1990)). Gene set enrichment analyses were performed on marginally significant genes using the subset of genes with known Entrez gene IDs against a background of all expressed genes using the clusterProfiler R Bioconductor package, which uses the hypergeometric test (Yu et al., 2012).

Cross-species enrichment analyses of the human SFARI (Banerjee-Basu and Packer, 2010) and Harmonizome (Rouillard et al., 2016) gene sets were performed with Fisher's exact tests (which is identical to the above hypergeometric test on these 2x2 enrichment tables) on the subsets of homologous and expressed genes in each mouse dataset. For SFARI analyses, we considered the sets of a) all genes in the mouse model database, b) all genes in the human gene database (N=1079 genes), c) only genes that were syndromic, or had gene scores of 1 or 2 (N=235 genes, which correspond to high-confidence genes) and d) only genes that had gene scores of 1 or 2, ignoring syndromic genes (N=91 genes). All RNA-seq analysis code is available on GitHub: https://github.com/LieberInstitute/cst_trap_seq.

Bulk cortex analysis for genotype effects

We used paired end read alignment and gene counting for these 10 samples (5 per genotype group). We analyzed 21,717 genes with reads per kilobase per million counted/assigned (RPKM normalizing to total number of gene counts, not mapped reads) greater than 0.1. We performed differential expression analysis with limma voom using genotype as the main outcome of interest, further adjusting for the gene assignment rate (measured by featureCounts), the chrM mapping rate, and one surrogate variable.

Input versus IP analysis

We used paired end read alignment and gene counting for these 6 samples (3 input and 3 IP). We analyzed 21,776 genes with RPKM > 0.1. We performed differential expression analysis with limma voom using fraction (IP vs. Input) as the main outcome of interest, further adjusting for the gene assignment rate (measured by featureCounts) and also using the duplicateCorrelation function in limma to treat each mouse as a random intercept by employing linear mixed effects modeling.

IP analysis for genotype effects

We used single end read alignment and gene counting for these 12 samples (6 per genotype). We analyzed 21,187 genes with RPKM > 0.1. We performed differential expression analysis with limma voom using genotype as the main outcome of interest, further adjusting for the gene assignment rate (measured by featureCounts).

RESULTS

Disruption of BDNF-TrkB signaling in Cort interneurons alters cortical gene expression

Mice with selective depletion of TrkB in Cort-expressing interneurons ($Cort^{Cre}$; $TrkB^{flox/flox}$, **Fig. 1*A***) develop spontaneous seizures at ~P21 (Hill et al., 2019). To better understand the molecular mechanisms downstream of TrkB signaling disruption in Cort interneurons that leads to hyperexcitability and disruption of excitatory/inhibitory balance, we performed bulk RNA

316 sequencing (RNA-seq) on the cortices of P21 Cort^{Cre}; TrkB$^{flox/flox}$ (n=5) and littermate controls (n=5).
317 Among the 21,717 expressed genes (at RPKM > 0.1), we identified 33 differentially expressed
318 between Cort^{Cre}; TrkB$^{flox/flox}$ and controls at FDR < 0.1 including 15 genes with absolute fold
319 changes greater than 2 (**Fig. 1*B*, Extended data Figure 1-1**). Of particular interest, we observed
320 increased expression of genes involved in cortical excitability such as tenomodulin (*Tnmd*,
321 encoding an angiogenesis inhibitor implicated in Alzheimer's (Tolppanen et al., 2011)),
322 neuropeptide Y (*Npy,* encoding a neuropeptide synthesized by GABAergic interneurons
323 (Karagiannis et al., 2009)), and calsenilin (*Kcnip3*, encoding a calcium binding protein that
324 influences cortical excitability (Pruunsild and Timmusk, 2005); 5.06, 1.68, and 1.52 fold changes,
325 respectively, p=1.7 x 10^{-6}, 2.24 x 10^{-5}, 1.26 x 10^{-4}). We also observed decreased expression of
326 ATPase plasma membrane Ca2+ transporting 4 (*Atp2b4)*, matrilin 2 (*Matn2)*, and cholinergic
327 receptor nicotinic alpha 4 subunit (*Chrna4*; 1.48, 1.57, and 1.49 fold changes, respectively, p =
328 1.46 x 10^{-4}, 2.1 × 10^{-5}, and 3.68 × 10^{-5} respectively). These genes encode proteins that are
329 important for intracellular calcium homeostasis, formation of filamentous networks in the
330 extracellular matrix, and acetylcholine signaling, respectively (Kuryatov et al., 1997; Mates et al.,
331 2002; Ho et al., 2015). To independently validate RNA-seq results, we confirmed differential
332 expression of a subset of up- and down-regulated genes using qPCR. We verified significant
333 elevation of secretogranin II (*Scg2,*) and neuronal pentraxin II (*Nptx2*), additional genes of interest
334 due to their roles in packaging neuropeptides into secretory vesicles and excitatory synapse
335 formation, in Cort^{Cre}; TrkB$^{flox/flox}$ compared to control mice (1.5 and 2 fold changes, p < 0.5 and
336 0.001, respectively; **Fig. 1*D*;** (Ozawa and Takata, 1995; O'Brien et al., 1999). We also validated
337 reduction of *Chrna4* and *Matn2* transcripts (0.6 and 0.5 fold changes, p < 0.001 and 0.0001
338 respectively; **Fig. 1*D***).

339 To identify signaling pathways impacted by differentially expressed genes in Cort^{Cre};
340 TrkB$^{flox/flox}$ cortex compared to control, we performed Gene Ontology (GO) analysis on the subset of
341 269 marginally significant (at p <0.005) genes with Entrez gene IDs, stratified by directionality (133

more highly expressed in control and 136 more highly expressed in Cort^{Cre}; TrkB$^{flox/flox}$; **Fig. 1*C*;** **Extended Data Figure 1-2**). Consistent with the hyperexcitability phenotype in Cort^{Cre}; TrkB$^{flox/flox}$ mice, analysis with the cellular component category showed terms such as glutamatergic synapse ($p= 3.69 \times 10^{-5}$), neuron projection terminus ($p= 2.63 \times 10^{-4}$), and collagen-containing extracellular matrix ($p= 3.06 \times 10^{-8}$). Analysis with the molecular function category showed terms such as calcium ion transmembrane transporter activity ($p= 4.75 \times 10^{-4}$), glutamate receptor activity ($p= 1.35 \times 10^{-3}$), and excitatory extracellular ligand-gated ion channel activity ($p= 1.52 \times 10^{-3}$). Analysis with the biological processes category showed terms such as positive chemotaxis ($p= 3.07 \times 10^{-4}$), calcium ion regulated exocytosis ($p= 6.67 \times 10^{-4}$), and neurotransmitter-gated ion channel clustering ($p= 4.55 \times 10^{-4}$). Taken together, GO analysis of differentially expressed genes supports the hypothesis that disruption of BDNF-TrkB signaling in Cort interneurons impacts signaling pathways that control excitatory/inhibitory balance and network excitability.

Translatome profiling delineates a comprehensive molecular identity for Cort-expressing interneurons in the cortex

Given the critical role of Cort neurons in maintaining cortical excitatory/inhibitory balance, we sought to better understand the molecular profile of Cort neurons using translating ribosome affinity purification (TRAP) followed by RNA-seq. We first crossed mice expressing Cre recombinase under control of the cortistatin promoter (Cort^{Cre}) to mice expressing a Cre-dependent hemaglutinnin (HA) peptide tag on the RPL22 ribosomal subunit (Rpl22^{HA}; **Fig. 2*A***) to allow for HA-tagging of ribosomes selectively in Cort neurons. Tagged ribosomes were immunoprecipitated (IP) from cortical homogenate tissue (Input) using an anti-HA antibody. Ribosome-associated RNA was isolated from IP samples and total RNA was isolated from Input samples.

Cell type-specific expression of the RiboTag allele in Cort neurons was confirmed by qPCR analysis showing significant enrichment of *Cort* transcripts in IP compared to the Input fraction (~20 fold; $p<0.0001$; **Fig 2*B***). We also showed expected enrichment of glutamate decarboxylase 1

(*Gad1*) and depletion of glial fibrillary acidic protein (*Gfap)* and *Bdnf* exon IV-containing transcripts (6, 0.25, and 0.2 fold changes, p<0.01, =0.0707, and 0.0581 respectively; **Fig 2*B***; (Gorba and Wahle, 1999; Swanwick et al., 2004)). Having confirmed successful IP from Cort-expressing interneurons, we generated stranded, rRNA depleted low-input libraries from Input and IP fractions and performed RNA-seq. Among the 21,776 expressed genes (at RPKM > 0.1), we identified 868 differentially expressed between Input and IP RNA fractions at Bonferroni-corrected p-values < 0.05 (and 5,362 genes at FDR < 0.05), including 627 genes with absolute fold changes greater than 2 (**Fig. 2*C*; Extended Data Figure 2-1**). Reassuringly, differential expression analysis confirmed significant enrichment (IP/Input) of *Cort* transcripts (2.7 fold increase, $p = 3.93 \times 10^{-3}$) and significant depletion of transcripts for *Gfap, Mal* (T cell differentiation protein), *Slc25a18* (solute Carrier Family 25 Member 18) and *Bdnf*, genes enriched in astrocytes, oligodendrocytes, and excitatory neurons, respectively (Schaeren-Wiemers et al., 1995b; Zhou and Danbolt, 2014; Hol and Pekny, 2015; Sasi et al., 2017). To independently validate our RNA-seq results, we confirmed differential expression of a subset of enriched and de-enriched genes, including neurexophilin 1 (*Nxph1)*, synaptotagmin 2 (*Syt2*), tetratricopeptide repeat domain 9B (*Ttc9b*), and S100 calcium binding protein A10 (*S100a10*). These genes are of particular interest given their role in synapse function and calcium signaling (Pang et al., 2006; Svenningsson et al., 2013). Using qPCR, we verified significant enrichment of *Nxph1* and *Syt2* and de-enrichment of *Ttc9b* and *S100a10* in Cort IP compared to Input samples (7.0, 7.0, 0.2, and 0.1 fold changes, respectively p<0.0001) (**Fig. 2*E***). To further confirm these results, we performed cell type-specific expression analysis (CSEA) on the top 100 differentially expressed genes based on fold change. This analysis confirmed significant over-representation of transcripts expressed in Cort neurons (**Extended Data Figure 2-2;** (Xu et al., 2014)).

To discover potential functional significance of the mRNAs enriched and depleted in Cort-expressing interneurons in the cortex, we performed Gene Ontology (GO) analysis on the subset of 848 Bonferroni-significant genes differentially expressed in Cort IP compared to Input with

Entrez gene IDs, stratified by directionality (440 more highly expressed in IP, 408 more highly expressed in Input; **Fig. 2*D*; Extended Data Figure 2-3**). Genes enriched in IP fractions are involved in cellular component category terms such as axon part and neuron projection terminus and in biological process category terms such as synapse organization and cerebral cortex tangential migration. Genes enriched in Input fractions are involved in cellular component category terms such as myelin sheath and biological processes category terms such as gliogenesis. De-enrichment of myelin and gliogenesis pathways would be expected in the neuronal IP fractions, and hence further validate our approach.

Loss of BDNF-TrkB signaling in Cort interneurons impacts genes critical for structural and functional plasticity

To better understand signaling pathways and cellular functions modulated by BDNF-TrkB signaling in Cort cells, we performed TRAP followed by RNA-seq in TrkB-depleted Cort interneurons. We intercrossed $Cort^{Cre}$; $Rpl22^{HA}$ mice to mice expressing a floxed TrkB allele ($TrkB^{flox/flox}$) to allow for HA tagging of ribosomes in control Cort interneurons ($Cort^{Cre}$; $Rpl22^{HA}$) or TrkB-depleted Cort interneurons ($Cort^{Cre}$;$TrkB^{flox/flox}$;$Rpl22^{HA}$; **Fig. 3*A*).** For control and experimental animals (n=6 each), tagged ribosomes were selectively immunoprecipitated (IP) from cortical homogenate tissue (Input) using an anti-HA antibody. Ribosome-associated RNA was isolated from IP samples and total RNA was isolated from Input samples.

Cell type specific-expression of the RiboTag allele in Cort interneurons was confirmed by qPCR analysis showing significant enrichment of *Cort* in IP vs Input fractions (12-15 fold; $p<0.0001$; **Fig. 3*B***). As expected, there was also significant enrichment of *Gad1* (8-12 fold; $p<0.001$ for control, $p<0.0001$ for $Cort^{Cre}$;$TrkB^{flox/flox}$ mice; **Fig. 3*B***) and significant depletion of *Gfap* (0.2-0.3 fold; $p<0.01$ for both groups; **Fig. 3*B***) and *Bdnf* exon IV-containing transcripts (0.1-0.3 fold; $p<0.001$ for control, $p<0.05$ for $Cort^{Cre}$;$TrkB^{flox/flox}$ mice; **Fig. 3*B***). We generated libraries from control and $Cort^{Cre}$; $TrkB^{flox/flox}$;$Rpl22^{HA}$ IP fractions and performed RNA-seq to generate a

comprehensive molecular profile of genes enriched and depleted in TrkB-deficient Cort neurons. Among the 21,187 expressed genes (at RPKM > 0.1), we identified 444 differentially expressed between IP RNA fractions at FDR < 0.05, including 75 genes with fold changes greater than 2 (**Fig. 3*C*, Extended Data Figure 3-1).** Of particular interest, differential expression analysis confirmed significant enrichment ($Cort^{Cre}$; $Rpl22^{HA}$; $TrkB^{flox/flox}$ IP compared to control IP) of wilms tumor 1 (*Wt1)*, synaptotagmin 6 (*Syt6)*, and G protein subunit gamma 4 (*Gng4)* transcripts (5.45, 2.17, and 2.78 fold increase, $p=2.91 \times 10^{-4}$, 1.68 x 10^{-8}, 1.9 x 10^{-11}, respectively). We observed significant depletion of transcripts for the transient receptor potential cation channel subfamily C member 6 (*Trpc6)*, calbindin 1 (*Calb1*) and galectin 1 (*Lgals1)* transcripts (1.3, 2.69, 2.19, and 3.46 fold decrease, $p=2.93 \times 10^{-8}$, 2.13 x 10^{-9}, 1.3 x 10^{-13}, 2.55 x 10^{-9}, respectively). Several of these genes are of interest due to their involvement in calcium signaling/homeostasis (Butz et al., 1999; Li et al., 2012; Schmidt, 2012) and axon development (Kobayakawa et al., 2015): pathways identified to be perturbed in bulk cortex following BDNF-TrkB disruption in Cort neurons (**Fig. 1**).

To explore the functional significance of the mRNAs enriched and depleted in Cort interneurons with disrupted BDNF-TrkB signaling, we performed Gene Ontology (GO) analysis on the subset of 161 Entrez genes more highly expressed in TrkB-depleted Cort neurons and the 269 Entrez genes more highly expressed in control Cort neurons (**Fig. 3*D*; Extended Data Figure 3-2**). Terms in both the molecular function and biological processes categories showed that cortistatin interneurons with disrupted BDNF-TrkB signaling were depleted for calcium ion binding, cellular calcium ion homeostasis, and calcium ion transport (FDR< 0.05). Ion channel complex and axon part, two cellular component category terms, were both depleted and enriched in $Cort^{Cre}$;$TrkB^{flox/flox}$ interneurons, which indicates that disrupting BDNF-TrkB signaling modulates important cellular responses. For the biological process terms, positive regulation of neuron projection development and axon development were both enriched and depleted in those interneurons. Terms associated with both enrichment and depletion in Cort interneurons include different genes, which suggests that these cells may undergo gene-specific changes that support their ability to respond to different

446 cellular signaling pathways.Taken together, these results support the hypothesis that BDNF-TrkB
447 signaling regulates structural and functional plasticity in Cort interneurons to maintain
448 excitatory/inhibitory balance.

449 To independently validate RNA-seq hits, we used qPCR to confirm significant enrichment
450 and depletion of the above-mentioned transcripts in $Cort^{Cre}$; $TrkB^{flox/flox}$; $Rpl22^{HA}$ IP samples
451 compared to control IP samples**.** We showed significant enrichment of *Wt1*, *Syt6*, and *Gng4*
452 transcripts (3, 2.8, 2.9 fold changes, p<0.01, 0.001, 0.0001 respectively). Furthermore, we showed
453 significant depletion of *Trpc6*, *Calb1* and *Lgals1* transcripts (0.3, 0.5, and 0.25 fold changes,
454 p<0.001, 0.001, 0.0001; **Fig. 4*A*)**. We independently validated significant enrichment of *Wt1* using
455 single molecule fluorescent *in situ* hybridization in in TrkB-ablated Cort neurons ($Cort^{Cre}$; $TrkB^{flox/flox}$;
456 $Rpl22^{HA}$) compared to compared to control Cort neurons (p<0.0001, **Fig. 4*B-D*)**.
457
458 **Genes important for Cort neuron identity and function overlap with those identified in**
459 **Autism Spectrum Disorder**
460 Finally, we explored the potential clinical relevance of deficits in Cort neuron function using pre-
461 defined genes sets from autism sequencing studies (using SFARI) and disease ontologies (using
462 Harmonizome). We found no significant enrichment in our bulk RNA-seq data with those identified
463 in both Autism Spectrum Disorder (ASD) and animal models relevant for ASD by the Simons
464 Foundation Autism Research Initiative (SFARI) (Banerjee-Basu and Packer, 2010). However, we
465 found enrichment for ASD genes among those genes highly expressed in Cort interneurons
466 (**Extended Data Figure 3-3**). For example, of the 239 genes in the “Mouse models” SFARI
467 database expressed in our data, 27 (11.0%) were differentially expressed in Cort interneurons
468 compared to total cortex, constituting a 6.3 fold enrichment ($p=9.25 \times 10^{-13}$). Similarly, of the 937
469 genes in the “Human gene” SFARI database (which contains genes with rare variation associated
470 with ASD from sequencing studies) with homologs expressed in our data, 93 were differentially
471 expressed (9.9%, 4.2 fold enrichment, $p=9.03 \times 10^{-25}$). These enrichments were preserved in the

more stringent subset of ASD genes, either with (OR=5.71, p=8.98 x 10^{-14}) or without (OR=6.55, p=8.06 x 10^{-8}) syndromic genes (see Methods). We further found significant enrichment for the overlap of genes differentially expressed in TrkB-depleted Cort cells compared to control Cort cells with those identified in both human and animal models of ASD as identified by SFARI (**Extended Data Figure 3-3**). Here, of the 237 genes in the "Mouse models" SFARI database expressed in our data, 26 (11.0%) were differentially expressed in $Cort^{Cre}$;$TrkB^{flox/flox}$ mice compared to control, constituting a 6 fold enrichment (p=6.85 x 10^{-12}). Similarly, of the 917 genes in the "Human gene" SFARI database with homologs expressed in our data, 66 were differentially expressed (7.2%, 2.8 fold enrichment, p=3.06 x 10^{-11}), which were preserved in the smaller subset of more stringent ASD genes with (OR=2.83, p=0.002) or without (OR=2.68, p=0.02) syndromic genes (see Methods).

In addition to the overlap of ASD relevant genes with those important for Cort identity and function, there was significant enrichment of many gene sets related to psychiatric disorders (at both the diseases and endophenotype levels) in the Harmonizome database (Rouillard et al., 2016) with those sets of genes preferentially expressed in Cort neurons and those dysregulated following TrkB depletion (**Extended Data Figure 3-4**). In addition to enrichment for psychiatric disorders, we further found enrichment of epilepsy-related genes among TrkB-depleted and control Cort neurons (35 genes, p =1.93 x 10^{-12}, **Extended Data Figure 3-4).** Together, these results further implicate Cort neurons in several debilitating human brain disorders (Xu et al., 2014).

DISCUSSION

TrkB signaling in Cort interneurons regulates gene pathways that modulate cortical excitability.

To better understand how disrupting BDNF-TrkB signaling in Cort cells impairs cortical function, we performed bulk RNA-seq on cortical tissue derived from $Cort^{Cre}$;$TrkB^{flox/flox}$ and control mice and identified significant differential expression of genes important for excitatory neuron function. Pathway analysis of these differentially expressed genes revealed functions associated

with glutamatergic synapses and synaptic membranes (**Fig. 1*C***). For example, we observed altered expression of neuronal pentraxin II (*Nptx2,* log2FC=1.26, p=3.60x10^{-5}*)*, which encodes a synaptic protein implicated in excitatory synapse formation and neural plasticity (Gu et al., 2013) that is bidirectionally regulated by BDNF in hippocampal neurons both *in vitro* and *in vivo* (Mariga et al., 2015). Our dataset also shows increases in cAMP responsive element Binding Protein 3 Like 1, which is necessary and sufficient to activate *Nptx2* transcription after BDNF treatment (Mariga et al., 2015). The protein encoded by *Nptx2* is also directly implicated in BDNF-mediated modulation of glutamatergic synapses, where it facilitates targeting and stabilization of AMPA receptors on excitatory synapses (Chang et al., 2010; Martin and Finsterwald, 2011; Pelkey et al., 2015). *Npy* is another differentially expressed gene (log2FC=0.75, p=2.24 x10^{-5}) that influences cortical excitability by reducing excitatory transmission onto neurons in the lateral habenula (Cheon et al., 2019) and inhibiting glutamatergic synaptic transmission in the hippocampus (Xapelli et al., 2008). NPY expression can slow the spread of seizures and has neuroprotective effects against excitotoxicity via increased BDNF signaling (Richichi et al., 2004; Xapelli et al., 2008).

Bdnf transcripts are paradoxically upregulated when comparing Cort^{Cre}; TrkB$^{flox/flox}$ to controls in the bulk RNA-seq dataset (log2FC=0.95, p= 3.55 x 10^{-5}). Because TrkB receptors were selectively depleted from Cort interneurons, which do not synthesize BDNF (Gorba and Wahle, 1999; Swanwick et al., 2004), *Bdnf* increases likely result from upregulation in cortical excitatory neurons. *Bdnf* expression may be induced in excitatory neurons following loss of TrkB in Cort interneurons for several reasons. First, in Cort^{Cre}; TrkB$^{flox/flox}$ mice, impaired Cort interneuron function may facilitate disinhibition of excitatory neurons leading to increased cortical excitability and subsequent activity-induced *Bdnf* expression (Lu, 2003). Alternatively, increased *Bdnf* expression may be a compensatory mechanism attempting to counterbalance TrkB depletion in cortistatin cells. BDNF levels increase following seizures (Gall et al., 1991; Isackson et al., 1991; Mudo et al., 1996), and increases in BDNF can subsequently contribute to hyperexcitability and seizure propagation (Kokaia et al., 1995; Scharfman, 1997; Binder et al., 1999; Croll et al., 1999).

Therefore, initiation and progressive worsening of seizures seen in Cort^{Cre}; TrkB$^{flox/flox}$ mice could be exacerbated by increases in *Bdnf*. It should be noted that at the time of brain extraction (P21), mild seizures may have already begun and could be influencing gene expression. In summary, depletion of TrkB receptors from Cort inhibitory interneurons may disrupt inhibitory signaling, leading to disinhibition of cortical excitatory neurons and disruption of network activity. This imbalance may push the cortex towards elevated excitation and increased expression of activity-dependent genes such as *Bdnf*, *Nptx2*, and *Npy*.

Cortistatin neurons are enriched in genes relevant to ASD

Translatome profiling in Cort neurons showed enrichment of neuron-relevant genes such as *Syt2*, a synaptic vesicle membrane protein (Bornschein and Schmidt, 2018) and *Nxph1*, a protein important for dendrite-axon adhesion (Born et al., 2014). We also observed expected depletion of genes such as *Mal*, a gene implicated in myelination (Schaeren-Wiemers et al., 1995a) , and *Apoe*, which is synthesized in astrocytes (Holtzman et al., 2012). These data expand on a similar translatome profiling experiment previously performed by (Doyle et al., 2008) using different mouse models and methodology. In that study, investigators used a mouse in which the EGFP-L10a ribosomal fusion protein is expressed under control of the *Cort* promoter in a bacterial artificial chromosome, and gene expression data was obtained using a microarray approach combined with TRAP. Here, we used a mouse that expresses Cre from the endogenous *Cort* promoter and gene expression data were obtained using a Ribotag/RNA-seq approach. Reassuringly, there is significant overlap between the Doyle microarray dataset and our RNA-seq analysis (**Extended Data Figure 2-1)**.

Xu et al., 2014 showed candidate autism genes from human genetics studies are enriched in Cort cells, supporting the notion that cortical interneurons play a significant role in the etiology of ASD. Epilepsy, a common neurological disorder characterized by recurrent seizures, is highly comorbid with ASD (Viscidi et al., 2013) and it has been proposed that these disorders may have

550 overlapping genetic risk that points to shared underlying molecular and cellular mechanisms. Of
551 note, interneuron dysfunction has been identified as a potential shared cellular mechanism in
552 mouse models of both disorders (Jacob, 2016). Our results further demonstrate enrichment of
553 genes associated with epilepsy and ASD in Cort neurons and highlight differential expression of
554 several ASD and epilepsy genes in Cort neurons following disruption of TrkB signaling. Our
555 findings support the overlapping developmental origins of the two illnesses and highlight BDNF-
556 TrkB signaling as potentially relevant to their etiology.
557
558 **Genes associated with calcium signaling and axonal development are disrupted following**
559 **TrkB depletion in cortistatin interneurons**
560 To identify putative molecular mechanisms that contribute to Cort interneuron dysfunction in
561 $Cort^{Cre}$;$TrkB^{flox/flox}$ mice, we compared the translatomes of intact Cort interneurons and Cort
562 interneurons depleted of TrkB receptors. TrkB-depleted Cort neurons show dysregulation of genes
563 associated with calcium ion homeostasis (*Calb1*, calcium binding protein, (Schmidt, 2012)) or
564 calcium dependent functions (*Syt6*, calcium dependent exocytosis, (Fukuda et al., 2003)), as well
565 as genes associated with axon development (*Robo1*, axon guidance, (Andrews et al., 2006)) and
566 cell/cell or cell/matrix interactions (*Lgals1*, plasma membrane adhesion molecule, (Camby et al.,
567 2006)).
568 During development, cortical interneurons are generated in the ventral subcortical
569 telencephalon and travel long distances to reach their final destination in cortical circuits, both
570 tangentially from their birthplace in the ganglionic eminences and radially to their correct laminar
571 position (Cooper, 2013). Chemokine signaling is important for the transition from tangential to
572 radial migration and expression of chemokine receptors is directly affected by BDNF-TrkB signaling
573 in the central nervous system, as well as in disease states such as cancer (Azoulay et al., 2018).
574 We found that expression of *Cxcr4,* a chemokine receptor, is reduced in TrkB-depleted cortistatin
575 interneurons by a factor of 4, which supports previous work showing modulation of CXCR4

576 expression and receptor internalization by BDNF-TrkB signaling (Ahmed et al., 2008). Degradation
577 of this protein has been identified as a permissive signal for interneurons to leave tangential
578 migratory streams (Sanchez-Alcaniz et al., 2011). Deletion of the gene leads to defects in cortical
579 layer positioning (Li et al., 2008; Wang et al., 2011) and mutations result in premature
580 accumulation of interneurons in the cortex. Although laminar distribution of Cort cells does not
581 appear to be significantly altered by loss of TrkB (Hill et al., 2019), premature entry into the cortex
582 may result in incorrect integration into the circuitry or improper axonal projections that cannot be
583 inferred by laminar position. This explanation is further supported by altered expression of genes
584 associated with axonogenesis, axon guidance, neuron projection terminus, and cell matrix
585 interactions (**Fig. 3**). The fact that CXCR4 is normally expressed in axons and functions to define
586 their trajectory (Lieberam et al., 2005; Vilz et al., 2005; Miyasaka et al., 2007) provides additional
587 strength to this hypothesis. In addition to *Cxcr4*, calcium signaling is important for stimulating
588 (Behar et al., 1999) and halting (Bortone and Polleux, 2009) neuronal migration to the cortex, and
589 $Cort^{Cre}$;$TrkB^{flox/flox}$ mice show decreased expression of genes in calcium related GO categories
590 compared to control mice (**Fig. 3**), such as *Calb1*. Importantly, exogenous application of BDNF
591 induces elevation of intracellular calcium (Berninger et al., 1993; Marsh and Palfrey, 1996), and
592 endogenous BDNF signaling elicits calcium responses at synapses (Lang et al., 2007). Additional
593 work would be necessary to tease out the effects of interneuron migration, migratory stream
594 maintenance, and correct development of projections during embryonic development in these
595 mutant mice. An important future direction will be to evaluate the morphology of Cort neurons
596 following disruption of BDNF-TrkB signaling.

597 In summary, we provide evidence that loss of BDNF-TrkB signaling in Cort interneurons
598 leads to alterations in calcium signaling and axon development in these cells, which may contribute
599 to altered excitatory/inhibitory balance in the cortex. Several of the genes enriched in Cort neurons
600 and differentially expressed in TrkB-depleted neurons are implicated in both ASD and epilepsy.

These data shed light on the role of BDNF-TrkB signaling in the function of Cort-expressing interneurons and provide rationale for further functional studies of these interneurons.

REFERENCES

Ahmed F, Tessarollo L, Thiele C, Mocchetti I (2008) Brain-derived neurotrophic factor modulates expression of chemokine receptors in the brain. Brain research 1227:1-11.

Alcantara S, Pozas E, Ibanez CF, Soriano E (2006) BDNF-modulated spatial organization of Cajal-Retzius and GABAergic neurons in the marginal zone plays a role in the development of cortical organization. Cerebral cortex 16:487-499.

Andrews W, Liapi A, Plachez C, Camurri L, Zhang J, Mori S, Murakami F, Parnavelas JG, Sundaresan V, Richards LJ (2006) Robo1 regulates the development of major axon tracts and interneuron migration in the forebrain. Development 133:2243-2252.

Azoulay D, Herishanu Y, Shapiro M, Brandshaft Y, Suriu C, Akria L, Braester A (2018) Elevated serum BDNF levels are associated with favorable outcome in CLL patients: Possible link to CXCR4 downregulation. Experimental hematology 63:17-21 e11.

Banerjee-Basu S, Packer A (2010) SFARI Gene: an evolving database for the autism research community. Dis Model Mech 3:133-135.

Baydyuk M, Russell T, Liao GY, Zang K, An JJ, Reichardt LF, Xu B (2011) TrkB receptor controls striatal formation by regulating the number of newborn striatal neurons. Proceedings of the National Academy of Sciences of the United States of America 108:1669-1674.

Behar TN, Scott CA, Greene CL, Wen X, Smith SV, Maric D, Liu QY, Colton CA, Barker JL (1999) Glutamate acting at NMDA receptors stimulates embryonic cortical neuronal migration. The Journal of neuroscience : the official journal of the Society for Neuroscience 19:4449-4461.

Berninger B, Garcia DE, Inagaki N, Hahnel C, Lindholm D (1993) BDNF and NT-3 induce intracellular Ca2+ elevation in hippocampal neurones. Neuroreport 4:1303-1306.

626 Binder DK, Routbort MJ, Ryan TE, Yancopoulos GD, McNamara JO (1999) Selective inhibition of
627 kindling development by intraventricular administration of TrkB receptor body. The Journal
628 of neuroscience : the official journal of the Society for Neuroscience 19:1424-1436.
629 Born G, Breuer D, Wang S, Rohlmann A, Coulon P, Vakili P, Reissner C, Kiefer F, Heine M, Pape
630 HC, Missler M (2014) Modulation of synaptic function through the alpha-neurexin-specific
631 ligand neurexophilin-1. Proceedings of the National Academy of Sciences of the United
632 States of America 111:E1274-1283.
633 Bornschein G, Schmidt H (2018) Synaptotagmin Ca(2+) Sensors and Their Spatial Coupling to
634 Presynaptic Cav Channels in Central Cortical Synapses. Frontiers in molecular
635 neuroscience 11:494.
636 Bortone D, Polleux F (2009) KCC2 expression promotes the termination of cortical interneuron
637 migration in a voltage-sensitive calcium-dependent manner. Neuron 62:53-71.
638 Butz S, Fernandez-Chacon R, Schmitz F, Jahn R, Sudhof TC (1999) The subcellular localizations
639 of atypical synaptotagmins III and VI. Synaptotagmin III is enriched in synapses and
640 synaptic plasma membranes but not in synaptic vesicles. The Journal of biological
641 chemistry 274:18290-18296.
642 Camby I, Le Mercier M, Lefranc F, Kiss R (2006) Galectin-1: a small protein with major functions.
643 Glycobiology 16:137R-157R.
644 Cellerino A, Maffei L, Domenici L (1996) The distribution of brain-derived neurotrophic factor and
645 its receptor trkB in parvalbumin-containing neurons of the rat visual cortex. The European
646 journal of neuroscience 8:1190-1197.
647 Chang MC, Park JM, Pelkey KA, Grabenstatter HL, Xu D, Linden DJ, Sutula TP, McBain CJ,
648 Worley PF (2010) Narp regulates homeostatic scaling of excitatory synapses on
649 parvalbumin-expressing interneurons. Nature neuroscience 13:1090-1097.
650 Cheon M, Park H, Rhim H, Chung C (2019) Actions of Neuropeptide Y on Synaptic Transmission
651 in the Lateral Habenula. Neuroscience.

652 Colliva A, Maynard KR, Martinowich K, Tongiorgi E (2018) Detecting Single and Multiple BDNF
653 Transcripts by In Situ Hybridization in Neuronal Cultures and Brain Sections. Humana
654 Press:1-27.
655 Cooper JA (2013) Cell biology in neuroscience: mechanisms of cell migration in the nervous
656 system. The Journal of cell biology 202:725-734.
657 Croll SD, Suri C, Compton DL, Simmons MV, Yancopoulos GD, Lindsay RM, Wiegand SJ, Rudge
658 JS, Scharfman HE (1999) Brain-derived neurotrophic factor transgenic mice exhibit passive
659 avoidance deficits, increased seizure severity and in vitro hyperexcitability in the
660 hippocampus and entorhinal cortex. Neuroscience 93:1491-1506.
661 Csaba Z, Dournaud P (2001) Cellular biology of somatostatin receptors. Neuropeptides 35:1-23.
662 de Lecea L, del Rio JA, Criado JR, Alcantara S, Morales M, Danielson PE, Henriksen SJ, Soriano
663 E, Sutcliffe JG (1997) Cortistatin is expressed in a distinct subset of cortical interneurons.
664 The Journal of neuroscience : the official journal of the Society for Neuroscience 17:5868-
665 5880.
666 de Lecea L, Criado JR, Prospero-Garcia O, Gautvik KM, Schweitzer P, Danielson PE, Dunlop CL,
667 Siggins GR, Henriksen SJ, Sutcliffe JG (1996) A cortical neuropeptide with neuronal
668 depressant and sleep-modulating properties. Nature 381:242-245.
669 Doyle JP, Dougherty JD, Heiman M, Schmidt EF, Stevens TR, Ma G, Bupp S, Shrestha P, Shah
670 RD, Doughty ML, Gong S, Greengard P, Heintz N (2008) Application of a translational
671 profiling approach for the comparative analysis of CNS cell types. Cell 135:749-762.
672 Fukuda M, Kanno E, Ogata Y, Saegusa C, Kim T, Loh YP, Yamamoto A (2003) Nerve growth
673 factor-dependent sorting of synaptotagmin IV protein to mature dense-core vesicles that
674 undergo calcium-dependent exocytosis in PC12 cells. The Journal of biological chemistry
675 278:3220-3226.

Gall C, Lauterborn J, Bundman M, Murray K, Isackson P (1991) Seizures and the regulation of neurotrophic factor and neuropeptide gene expression in brain. Epilepsy research Supplement 4:225-245.

Glorioso C, Sabatini M, Unger T, Hashimoto T, Monteggia LM, Lewis DA, Mirnics K (2006) Specificity and timing of neocortical transcriptome changes in response to BDNF gene ablation during embryogenesis or adulthood. Molecular psychiatry 11:633-648.

Gorba T, Wahle P (1999) Expression of TrkB and TrkC but not BDNF mRNA in neurochemically identified interneurons in rat visual cortex in vivo and in organotypic cultures. The European journal of neuroscience 11:1179-1190.

Grishanin RN, Yang H, Liu X, Donohue-Rolfe K, Nune GC, Zang K, Xu B, Duncan JL, Lavail MM, Copenhagen DR, Reichardt LF (2008) Retinal TrkB receptors regulate neural development in the inner, but not outer, retina. Molecular and cellular neurosciences 38:431-443.

Gu Y, Huang S, Chang MC, Worley P, Kirkwood A, Quinlan EM (2013) Obligatory role for the immediate early gene NARP in critical period plasticity. Neuron 79:335-346.

Guilloux JP, Douillard-Guilloux G, Kota R, Wang X, Gardier AM, Martinowich K, Tseng GC, Lewis DA, Sibille E (2012) Molecular evidence for BDNF- and GABA-related dysfunctions in the amygdala of female subjects with major depression. Molecular psychiatry 17:1130-1142.

Habib N, Avraham-Davidi I, Basu A, Burks T, Shekhar K, Hofree M, Choudhury SR, Aguet F, Gelfand E, Ardlie K, Weitz DA, Rozenblatt-Rosen O, Zhang F, Regev A (2017) Massively parallel single-nucleus RNA-seq with DroNc-seq. Nature methods 14:955-958.

Hill JL, Jimenez DV, Mai Y, Ren M, Hallock HL, Maynard KR, Chen HY, Hardy NF, Schloesser RJ, Maher BJ, Yang F, Martinowich K (2019) Cortistatin-expressing interneurons require TrkB signaling to suppress neural hyper-excitability. Brain structure & function 224:471-483.

Ho PW, Pang SY, Li M, Tse ZH, Kung MH, Sham PC, Ho SL (2015) PMCA4 (ATP2B4) mutation in familial spastic paraplegia causes delay in intracellular calcium extrusion. Brain and behavior 5:e00321.

Hodneland E, Kogel T, Frei DM, Gerdes HH, Lundervold A (2013) CellSegm - a MATLAB toolbox for high-throughput 3D cell segmentation. Source code for biology and medicine 8:16.

Hol EM, Pekny M (2015) Glial fibrillary acidic protein (GFAP) and the astrocyte intermediate filament system in diseases of the central nervous system. Current opinion in cell biology 32:121-130.

Holtzman DM, Herz J, Bu G (2012) Apolipoprotein E and apolipoprotein E receptors: normal biology and roles in Alzheimer disease. Cold Spring Harbor perspectives in medicine 2:a006312.

Huang ZJ, Kirkwood A, Pizzorusso T, Porciatti V, Morales B, Bear MF, Maffei L, Tonegawa S (1999) BDNF regulates the maturation of inhibition and the critical period of plasticity in mouse visual cortex. Cell 98:739-755.

Isackson PJ, Huntsman MM, Murray KD, Gall CM (1991) BDNF mRNA expression is increased in adult rat forebrain after limbic seizures: temporal patterns of induction distinct from NGF. Neuron 6:937-948.

Jacob J (2016) Cortical interneuron dysfunction in epilepsy associated with autism spectrum disorders. Epilepsia 57:182-193.

Karagiannis A, Gallopin T, David C, Battaglia D, Geoffroy H, Rossier J, Hillman EM, Staiger JF, Cauli B (2009) Classification of NPY-expressing neocortical interneurons. The Journal of neuroscience : the official journal of the Society for Neuroscience 29:3642-3659.

Kasen S, Ouellette R, Cohen P (1990) Mainstreaming and postsecondary educational and employment status of a rubella cohort. American annals of the deaf 135:22-26.

Katoh-Semba R, Takeuchi IK, Semba R, Kato K (1997) Distribution of brain-derived neurotrophic factor in rats and its changes with development in the brain. Journal of neurochemistry 69:34-42.

Kim D, Langmead B, Salzberg SL (2015) HISAT: a fast spliced aligner with low memory requirements. Nature methods 12:357-360.

728 Kobayakawa Y, Sakumi K, Kajitani K, Kadoya T, Horie H, Kira J, Nakabeppu Y (2015) Galectin-1
729 deficiency improves axonal swelling of motor neurones in SOD1(G93A) transgenic mice.
730 Neuropathology and applied neurobiology 41:227-244.
731 Kokaia M, Ernfors P, Kokaia Z, Elmer E, Jaenisch R, Lindvall O (1995) Suppressed
732 epileptogenesis in BDNF mutant mice. Experimental neurology 133:215-224.
733 Kuryatov A, Gerzanich V, Nelson M, Olale F, Lindstrom J (1997) Mutation causing autosomal
734 dominant nocturnal frontal lobe epilepsy alters Ca2+ permeability, conductance, and gating
735 of human alpha4beta2 nicotinic acetylcholine receptors. The Journal of neuroscience : the
736 official journal of the Society for Neuroscience 17:9035-9047.
737 Lang SB, Stein V, Bonhoeffer T, Lohmann C (2007) Endogenous brain-derived neurotrophic factor
738 triggers fast calcium transients at synapses in developing dendrites. The Journal of
739 neuroscience : the official journal of the Society for Neuroscience 27:1097-1105.
740 Law CW, Chen Y, Shi W, Smyth GK (2014) voom: Precision weights unlock linear model analysis
741 tools for RNA-seq read counts. Genome biology 15:R29.
742 Li G, Adesnik H, Li J, Long J, Nicoll RA, Rubenstein JL, Pleasure SJ (2008) Regional distribution of
743 cortical interneurons and development of inhibitory tone are regulated by Cxcl12/Cxcr4
744 signaling. The Journal of neuroscience : the official journal of the Society for Neuroscience
745 28:1085-1098.
746 Li H, Huang J, Du W, Jia C, Yao H, Wang Y (2012) TRPC6 inhibited NMDA receptor activities and
747 protected neurons from ischemic excitotoxicity. Journal of neurochemistry 123:1010-1018.
748 Liao Y, Smyth GK, Shi W (2014) featureCounts: an efficient general purpose program for assigning
749 sequence reads to genomic features. Bioinformatics 30:923-930.
750 Lieberam I, Agalliu D, Nagasawa T, Ericson J, Jessell TM (2005) A Cxcl12-CXCR4 chemokine
751 signaling pathway defines the initial trajectory of mammalian motor axons. Neuron 47:667-
752 679.
753 Lu B (2003) BDNF and activity-dependent synaptic modulation. Learning & memory 10:86-98.

754 Mariga A, Glaser J, Mathias L, Xu D, Xiao M, Worley P, Ninan I, Chao MV (2015) Definition of a
755 Bidirectional Activity-Dependent Pathway Involving BDNF and Narp. Cell reports 13:1747-
756 1756.
757 Marsh HN, Palfrey HC (1996) Neurotrophin-3 and brain-derived neurotrophic factor activate
758 multiple signal transduction events but are not survival factors for hippocampal pyramidal
759 neurons. Journal of neurochemistry 67:952-963.
760 Martin JL, Finsterwald C (2011) Cooperation between BDNF and glutamate in the regulation of
761 synaptic transmission and neuronal development. Communicative & integrative biology
762 4:14-16.
763 Martinowich K, Schloesser RJ, Jimenez DV, Weinberger DR, Lu B (2011) Activity-dependent brain-
764 derived neurotrophic factor expression regulates cortistatin-interneurons and sleep
765 behavior. Molecular brain 4:11.
766 Marty S, Berninger B, Carroll P, Thoenen H (1996) GABAergic stimulation regulates the phenotype
767 of hippocampal interneurons through the regulation of brain-derived neurotrophic factor.
768 Neuron 16:565-570.
769 Mates L, Korpos E, Deak F, Liu Z, Beier DR, Aszodi A, Kiss I (2002) Comparative analysis of the
770 mouse and human genes (Matn2 and MATN2) for matrilin-2, a filament-forming protein
771 widely distributed in extracellular matrices. Matrix biology : journal of the International
772 Society for Matrix Biology 21:163-174.
773 Meyer HS, Schwarz D, Wimmer VC, Schmitt AC, Kerr JN, Sakmann B, Helmstaedter M (2011)
774 Inhibitory interneurons in a cortical column form hot zones of inhibition in layers 2 and 5A.
775 Proceedings of the National Academy of Sciences of the United States of America
776 108:16807-16812.
777 Miyasaka N, Knaut H, Yoshihara Y (2007) Cxcl12/Cxcr4 chemokine signaling is required for
778 placode assembly and sensory axon pathfinding in the zebrafish olfactory system.
779 Development 134:2459-2468.

780 Mudo G, Jiang XH, Timmusk T, Bindoni M, Belluardo N (1996) Change in neurotrophins and their
781 receptor mRNAs in the rat forebrain after status epilepticus induced by pilocarpine.
782 Epilepsia 37:198-207.
783 Myers AJ et al. (2007) A survey of genetic human cortical gene expression. Nature genetics
784 39:1494-1499.
785 Nieto-Gonzalez JL, Jensen K (2013) BDNF Depresses Excitability of Parvalbumin-Positive
786 Interneurons through an M-Like Current in Rat Dentate Gyrus. PloS one 8:e67318.
787 O'Brien RJ, Xu D, Petralia RS, Steward O, Huganir RL, Worley P (1999) Synaptic clustering of
788 AMPA receptors by the extracellular immediate-early gene product Narp. Neuron 23:309-
789 323.
790 Ozawa H, Takata K (1995) The granin family--its role in sorting and secretory granule formation.
791 Cell structure and function 20:415-420.
792 Pang ZP, Melicoff E, Padgett D, Liu Y, Teich AF, Dickey BF, Lin W, Adachi R, Sudhof TC (2006)
793 Synaptotagmin-2 is essential for survival and contributes to Ca2+ triggering of
794 neurotransmitter release in central and neuromuscular synapses. The Journal of
795 neuroscience : the official journal of the Society for Neuroscience 26:13493-13504.
796 Pelkey KA, Barksdale E, Craig MT, Yuan X, Sukumaran M, Vargish GA, Mitchell RM, Wyeth MS,
797 Petralia RS, Chittajallu R, Karlsson RM, Cameron HA, Murata Y, Colonnese MT, Worley
798 PF, McBain CJ (2015) Pentraxins coordinate excitatory synapse maturation and circuit
799 integration of parvalbumin interneurons. Neuron 85:1257-1272.
800 Pruunsild P, Timmusk T (2005) Structure, alternative splicing, and expression of the human and
801 mouse KCNIP gene family. Genomics 86:581-593.
802 Richichi C, Lin EJ, Stefanin D, Colella D, Ravizza T, Grignaschi G, Veglianese P, Sperk G, During
803 MJ, Vezzani A (2004) Anticonvulsant and antiepileptogenic effects mediated by adeno-
804 associated virus vector neuropeptide Y expression in the rat hippocampus. The Journal of
805 neuroscience : the official journal of the Society for Neuroscience 24:3051-3059.

806 Ritchie ME, Phipson B, Wu D, Hu Y, Law CW, Shi W, Smyth GK (2015) limma powers differential
807 expression analyses for RNA-sequencing and microarray studies. Nucleic acids research
808 43:e47.
809 Rouillard AD, Gundersen GW, Fernandez NF, Wang Z, Monteiro CD, McDermott MG, Ma'ayan A
810 (2016) The harmonizome: a collection of processed datasets gathered to serve and mine
811 knowledge about genes and proteins. Database (Oxford) 2016.
812 Sanchez-Alcaniz JA, Haege S, Mueller W, Pla R, Mackay F, Schulz S, Lopez-Bendito G, Stumm R,
813 Marin O (2011) Cxcr7 controls neuronal migration by regulating chemokine responsiveness.
814 Neuron 69:77-90.
815 Sanz E, Yang L, Su T, Morris DR, McKnight GS, Amieux PS (2009) Cell-type-specific isolation of
816 ribosome-associated mRNA from complex tissues. Proceedings of the National Academy of
817 Sciences of the United States of America 106:13939-13944.
818 Sanz E, Evanoff R, Quintana A, Evans E, Miller JA, Ko C, Amieux PS, Griswold MD, McKnight GS
819 (2013) RiboTag analysis of actively translated mRNAs in Sertoli and Leydig cells in vivo.
820 PloS one 8:e66179.
821 Sasi M, Vignoli B, Canossa M, Blum R (2017) Neurobiology of local and intercellular BDNF
822 signaling. Pflugers Archiv : European journal of physiology 469:593-610.
823 Schaeren-Wiemers N, Valenzuela DM, Frank M, Schwab ME (1995a) Characterization of a rat
824 gene, rMAL, encoding a protein with four hydrophobic domains in central and peripheral
825 myelin. The Journal of neuroscience : the official journal of the Society for Neuroscience
826 15:5753-5764.
827 Schaeren-Wiemers N, Schaefer C, Valenzuela DM, Yancopoulos GD, Schwab ME (1995b)
828 Identification of new oligodendrocyte- and myelin-specific genes by a differential screening
829 approach. Journal of neurochemistry 65:10-22.
830 Scharfman HE (1997) Hyperexcitability in combined entorhinal/hippocampal slices of adult rat after
831 exposure to brain-derived neurotrophic factor. Journal of neurophysiology 78:1082-1095.

832 Schmidt H (2012) Three functional facets of calbindin D-28k. Frontiers in molecular neuroscience
833 5:25.
834 Schweitzer P, Madamba SG, Siggins GR (2003) The sleep-modulating peptide cortistatin
835 augments the h-current in hippocampal neurons. The Journal of neuroscience : the official
836 journal of the Society for Neuroscience 23:10884-10891.
837 Somogyi J, Baude A, Omori Y, Shimizu H, El Mestikawy S, Fukaya M, Shigemoto R, Watanabe M,
838 Somogyi P (2004) GABAergic basket cells expressing cholecystokinin contain vesicular
839 glutamate transporter type 3 (VGLUT3) in their synaptic terminals in hippocampus and
840 isocortex of the rat. The European journal of neuroscience 19:552-569.
841 Souza-Moreira L, Morell M, Delgado-Maroto V, Pedreno M, Martinez-Escudero L, Caro M, O'Valle
842 F, Luque R, Gallo M, de Lecea L, Castano JP, Gonzalez-Rey E (2013) Paradoxical effect of
843 cortistatin treatment and its deficiency on experimental autoimmune encephalomyelitis.
844 Journal of immunology 191:2144-2154.
845 Svenningsson P, Kim Y, Warner-Schmidt J, Oh YS, Greengard P (2013) p11 and its role in
846 depression and therapeutic responses to antidepressants. Nature reviews Neuroscience
847 14:673-680.
848 Swanwick CC, Harrison MB, Kapur J (2004) Synaptic and extrasynaptic localization of brain-
849 derived neurotrophic factor and the tyrosine kinase B receptor in cultured hippocampal
850 neurons. The Journal of comparative neurology 478:405-417.
851 Taniguchi H, He M, Wu P, Kim S, Paik R, Sugino K, Kvitsiani D, Fu Y, Lu J, Lin Y, Miyoshi G,
852 Shima Y, Fishell G, Nelson SB, Huang ZJ (2011) A resource of Cre driver lines for genetic
853 targeting of GABAergic neurons in cerebral cortex. Neuron 71:995-1013.
854 Tolppanen AM, Helisalmi S, Hiltunen M, Kolehmainen M, Schwab U, Pirttila T, Pulkkinen L,
855 Uusitupa M, Soininen H (2011) Tenomodulin variants, APOE and Alzheimer's disease in a
856 Finnish case-control cohort. Neurobiology of aging 32:546 e547-549.

857 Tremblay R, Lee S, Rudy B (2016) GABAergic Interneurons in the Neocortex: From Cellular
858 Properties to Circuits. Neuron 91:260-292.
859 van Diessen E, Senders J, Jansen FE, Boersma M, Bruining H (2015) Increased power of resting-
860 state gamma oscillations in autism spectrum disorder detected by routine
861 electroencephalography. European archives of psychiatry and clinical neuroscience
862 265:537-540.
863 Veber DF, Holly FW, Nutt RF, Bergstrand SJ, Brady SF, Hirschmann R, Glitzer MS, Saperstein R
864 (1979) Highly active cyclic and bicyclic somatostatin analogues of reduced ring size. Nature
865 280:512-514.
866 Vilz TO, Moepps B, Engele J, Molly S, Littman DR, Schilling K (2005) The SDF-1/CXCR4 pathway
867 and the development of the cerebellar system. The European journal of neuroscience
868 22:1831-1839.
869 Viscidi EW, Triche EW, Pescosolido MF, McLean RL, Joseph RM, Spence SJ, Morrow EM (2013)
870 Clinical characteristics of children with autism spectrum disorder and co-occurring epilepsy.
871 PloS one 8:e67797.
872 Wang J, Barstein J, Ethridge LE, Mosconi MW, Takarae Y, Sweeney JA (2013) Resting state EEG
873 abnormalities in autism spectrum disorders. Journal of neurodevelopmental disorders 5:24.
874 Wang Y, Li G, Stanco A, Long JE, Crawford D, Potter GB, Pleasure SJ, Behrens T, Rubenstein JL
875 (2011) CXCR4 and CXCR7 have distinct functions in regulating interneuron migration.
876 Neuron 69:61-76.
877 Xapelli S, Bernardino L, Ferreira R, Grade S, Silva AP, Salgado JR, Cavadas C, Grouzmann E,
878 Poulsen FR, Jakobsen B, Oliveira CR, Zimmer J, Malva JO (2008) Interaction between
879 neuropeptide Y (NPY) and brain-derived neurotrophic factor in NPY-mediated
880 neuroprotection against excitotoxicity: a role for microglia. The European journal of
881 neuroscience 27:2089-2102.

Xu X, Wells AB, O'Brien DR, Nehorai A, Dougherty JD (2014) Cell type-specific expression analysis to identify putative cellular mechanisms for neurogenetic disorders. The Journal of neuroscience : the official journal of the Society for Neuroscience 34:1420-1431.

Yamada MK, Nakanishi K, Ohba S, Nakamura T, Ikegaya Y, Nishiyama N, Matsuki N (2002) Brain-derived neurotrophic factor promotes the maturation of GABAergic mechanisms in cultured hippocampal neurons. The Journal of neuroscience : the official journal of the Society for Neuroscience 22:7580-7585.

Yu G, Wang LG, Han Y, He QY (2012) clusterProfiler: an R package for comparing biological themes among gene clusters. Omics : a journal of integrative biology 16:284-287.

Zhou Y, Danbolt NC (2014) Glutamate as a neurotransmitter in the healthy brain. Journal of neural transmission 121:799-817.

CONFLICT OF INTEREST

The authors declare no competing financial interests.

LEGENDS

Figure 1: Loss of TrkB signaling in Cort interneurons causes gene expression changes in pathways regulating excitability. A Schematic of control and $Cort^{Cre}$; $TrkB^{flox/flox}$ mice. **B** Volcano plot of bulk homogenate RNA-seq results with $Cort^{Cre}$; $TrkB^{flox/flox}$ vs. $Cort^{Cre}$ log_2 fold change against $-log_{10}$ p-value. Orange dots represent genes that are significantly different in $Cort^{Cre}$; $TrkB^{flox/flox}$ vs. $Cort^{Cre}$, including *Npy*, *Syt12*, *Nptx2*, and *Chrna4*. Green dots represent non-significant genes. See Extended Data Figure 1-1. **C** Gene ontology (GO) terms in the molecular function, biological processes, and cellular component categories for genes enriched and de-enriched in cortical tissue following ablation of TrkB in Cort neurons. See Extended Data Figure 1-2. **D** qPCR analysis validating genes found to be differentially expressed in bulk cortical

907 homogenate RNAseq of Cort^{Cre}; TrkB$^{flox/flox}$ vs. Cort^{Cre} mice (n=5 per genotype, student's unpaired
908 t-test, data presented as mean ± SEM *p<0.05 ***p<0.001 ****p<0.0001 vs. control).
909
910 **Figure 2: Translating ribosome affinity purification defines a unique molecular signature for**
911 **cortistatin interneurons in the cortex.** **A** Locus of the ribosomal protein Rpl22 in the RiboTag
912 mouse and breeding strategy used to obtain Cort^{Cre};Rpl22^{HA} mice. Schematic of RiboTag
913 experimental workflow. **B** Validation of RiboTag allele expression in cortistatin neurons by qPCR
914 for *Cort* as well as *Gad*, *Gfap*, and *Bdnf exon IV* (n=3 per genotype, student's unpaired t-test, data
915 presented as mean ± SEM **p<0.01 ****p<0.0001 vs. control). **C** Volcano plot of RNA-seq results
916 with Cort^{Cre};Rpl22^{HA} Input vs. Cort^{Cre};Rpl22^{HA} IP $\log_2$ fold change against $-\log_{10}$ p-value. Orange
917 dots represent genes that are significantly different in Input vs. IP fractions, including *Syt2*, *Nxph1*,
918 *Mal*, and *Apoe*. Green dots represent non-significant genes. See Extended Data Figures 2-1 and
919 2-2. **D** Gene ontology (GO) terms in the molecular function, biological processes, and cellular
920 component categories for genes enriched and de-enriched in Cort-expressing interneurons. See
921 Extended Data Figure 2-3. **E** qPCR analysis validating genes found to be differentially expressed
922 in Input vs. IP RNA sequencing results (n=3 per genotype, student's unpaired t-test, data
923 presented as mean ± SEM ****p<0.0001 vs. control).
924
925 **Figure 3: Loss of TrkB signaling in Cort neurons alters expression of genes important for**
926 **calcium homeostasis and axon development.** **A** Breeding strategy used to obtain control
927 Cort^{Cre}; Rpl22^{HA} and experimental Cort^{Cre}; TrkB$^{flox/flox}$; Rpl22^{HA} mice. **B** Validation of Ribotag allele
928 expression in cortistatin cells of control and Cort^{Cre}; TrkB$^{flox/flox}$; Rpl22^{HA} mice by qPCR of *Cort* as
929 well as *Gad*, *Gfap*, and *Bdnf* exon *IV* (n=6 per genotype, student's unpaired t-test, data presented
930 as mean ± SEM *p<0.05 **p<0.01 ***p<0.001 ****p<0.0001 vs. control). **C** Volcano plot of RNA-seq
931 results with Cort^{Cre}; TrkB$^{flox/flox}$; Rpl22^{HA} IP vs Cort^{Cre}; Rpl22^{HA} IP $\log_2$ fold change against $-\log_{10}$ p-
932 value. Orange dots represent genes that are significantly different in Cort^{Cre}; TrkB$^{flox/flox}$; Rpl22^{HA} IP

vs Cort^{Cre}; Rpl22^{HA} IP, including *Wt1*, *Calb1*, *Lgals1*, *Trpc6*, *Syt6*, and *Gng4*. Green dots represent non-significant genes. See Extended Data Figure 3-1. **D** Gene ontology (GO) terms in the molecular function, biological processes, and cellular component categories for genes enriched and de-enriched in Cort neurons following removal of TrkB and disruption of BDNF-TrkB signaling. See Extended Data Figures 3-2, 3-3, and 3-4.

Figure 4: **Validation of select targets from Cort^{Cre}; Rpl22^{HA} vs. Cort^{Cre}; TrkB$^{flox/flox}$; Rpl22^{HA} RNA-seq using qPCR and single molecule fluorescent *in situ* hybridization. A** qPCR analysis validating select genes (*Trpc6*, *Calb1*, *Lgals1*, *Wt1*, *Syt6*, *Gng4*) found to be differentially expressed in Cort^{Cre}; TrkB$^{flox/flox}$; Rpl22^{HA} IP vs. Control IP RNA-seq data (n=6 per genotype, student's unpaired t-test, data presented as mean ± SEM **p<0.01 ***p<0.001 ****p<0.0001 vs. control). **B** Quantification of *Wt1* transcripts in Cre positive cells of Cort^{Cre}; TrkB$^{flox/flox}$; Rpl22^{HA} and Control mice. **C-D** Confocal z-projections of *Cre* and *Wt1* transcripts in the cortex from P21 Cort^{Cre}; Rpl22^{HA} (c) and Cort^{Cre}; TrkB$^{flox/flox}$; Rpl22^{HA} (d) mice visualized with RNAscope in situ hybridization. *Wt1* transcripts (green) are more enriched in Cort neurons of Cort^{Cre}; TrkB$^{flox/flox}$; Rpl22^{HA} than Cort^{Cre}; Rpl22^{HA} mice. Inset depicts higher magnification of nuclei highlighted by arrows. Scale bar in c and d is 10μm.

EXTENDED DATA LEGENDS

(Extended Data are attached as .CSV, .TIF, or .XLSX files)

Extended Data Figure 1-1. Differential gene expression analysis of Cort^{Cre} vs. Cort^{Cre}; TrkB$^{flox/flox}$ bulk cortex for all expressed genes. Columns represent Symbol (mouse gene symbol), logFC (log2 fold change comparing experimental to control animals; positive values indicate higher expression in experimental animals), t (moderated T-statistic [with empirical Bayes]), P.Value (corresponding p-value from t-statistic), adj.P.Val (Benjamani-Hochberg adjusted

p-value to control the false discover rate, FDR), B (log odds of differential expression signal), gene_type (gencode class of gene), EntrezID (Entrez Gene ID), AveExpr (Average expression on the log2[counts per million + 0.5] scale, Length (coding gene length), ensemblID (Ensembl gene ID).

Extended Data Figure 1-2. Gene Ontology analysis of differentially expressed genes between Cort^{Cre} vs. Cort^{Cre}; TrkB$^{flox/flox}$ bulk cortex. Columns represent Cluster (label for set of differentially expressed genes), ONTOLOGY (Gene Ontology type: CC = cell compartment, BP = biological process, MF = molecular function), ID (Gene Ontology ID), Description (Gene Ontology set description), GeneRatio (fraction of differentially expressed genes were in the GO set), BgRatio (fraction of differentially expressed genes that were not in the GO set), Pvalue (P-value resulting from hypergeometric test), p.adjust (Benjamini-Hochberg adjusted p-value [FDR]), qvalue (Storey adjusted p-value), geneID (gene symbols corresponding to the differentially expressed genes in the GO set [i.e. from GeneRatio above]), Count (number of differentially expressed genes in the GO set [numerator of GeneRatio, to avoid forced Excel conversion to dates from some fraction]).

Extended Data Figure 2-1. Differential gene expression analysis of Cort^{Cre} Input vs. IP for all expressed genes. Columns represent Symbol (mouse gene symbol), logFC (log2 fold change comparing IP to Input samples; positive values indicate higher expression in IP samples), t (moderated T-statistic [with empirical Bayes]), P.Value (corresponding p-value from t-statistic), adj.P.Val (Benjamani-Hochberg adjusted p-value to control the false discover rate, FDR), B (log odds of differential expression signal), gene_type (gencode class of gene), EntrezID (Entrez Gene ID), AveExpr (Average expression on the log2[counts per million + 0.5] scale, Length (coding gene length), ensemblID (Ensembl gene ID).

Extended Data Figure 2-2: Cell type-specific expression analysis (CSEA) of IP-enriched genes in Cort neurons. CSEA of IP-enriched genes identifies Cort interneurons. Bullseye plot of the output of CSEA reveals a substantial over-representation of Cort positive neuron cell transcripts at multiple pSI levels among those transcripts (n=100) found to be enriched in our IP samples from Cort neurons. Box highlights Cort positive neurons.

Extended Data Figure 2-3. Gene Ontology analysis of differentially expressed genes between Cort^{Cre} Input vs. Cort^{Cre} IP. Columns represent Cluster (label for set of differentially expressed genes), ONTOLOGY (Gene Ontology type: CC = cell compartment, BP = biological process, MF = molecular function), ID (Gene Ontology ID), Description (Gene Ontology set description), GeneRatio (fraction of differentially expressed genes were in the GO set), BgRatio (fraction of differentially expressed genes that were not in the GO set), Pvalue (P-value resulting from hypergeometric test), p.adjust (Benjamini-Hochberg adjusted p-value [FDR]), qvalue (Storey adjusted p-value), geneID (gene symbols corresponding to the differentially expressed genes in the GO set [i.e. from GeneRatio above]), Count (number of differentially expressed genes in the GO set [numerator of GeneRatio, to avoid forced Excel conversion to dates from some fraction]).

Extended Data Figure 3-1. Differential gene expression analysis of Cort^{Cre} IP vs. Cort^{Cre}; TrkB$^{flox/flox}$ IP for all expressed genes. Columns represent Symbol (mouse gene symbol), logFC (log2 fold change comparing experimental to control animals; positive values indicate higher expression in experimental samples), t (moderated T-statistic [with empirical Bayes]), P.Value (corresponding p-value from t-statistic), adj.P.Val (Benjamani-Hochberg adjusted p-value to control the false discover rate, FDR), B (log odds of differential expression signal), gene_type (gencode class of gene), EntrezID (Entrez Gene ID), AveExpr (Average expression on the log2[counts per million + 0.5] scale, Length (coding gene length), ensemblID (Ensembl gene ID).

Extended Data Figure 3-2. Gene Ontology analysis of differentially expressed genes between Cort^{Cre} IP vs. Cort^{Cre}; TrkB$^{flox/flox}$ IP. Columns represent Direction (+1 is upregulated in experimental compared to control, -1 is downregulated in experimental compared to control), Cluster (label for set of differentially expressed genes), ONTOLOGY (Gene Ontology type: CC = cell compartment, BP = biological process, MF = molecular function), ID (Gene Ontology ID), Description (Gene Ontology set description), GeneRatio (fraction of differentially expressed genes were in the GO set), BgRatio (fraction of differentially expressed genes that were not in the GO set), Pvalue (P-value resulting from hypergeometric test), p.adjust (Benjamini-Hochberg adjusted p-value [FDR]), qvalue (Storey adjusted p-value), geneID (gene symbols corresponding to the differentially expressed genes in the GO set [i.e. from GeneRatio above]), Count (number of differentially expressed genes in the GO set [numerator of GeneRatio, to avoid forced Excel conversion to dates from some fraction]).

Extended Data Figure 3-3. Cort-enriched and TrkB-dependent genes in SFARI. Rows indicate SFARI genes (from either the human or mouse model databases, described in the text) that were differentially expressed in at least one dataset (Cort^{Cre} vs. Cort^{Cre}; TrkB$^{flox/flox}$ bulk cortex; Cort^{Cre} Input vs. IP; or Cort^{Cre} IP vs. Cort^{Cre}; TrkB$^{flox/flox}$ IP). TRUE indicates that gene was significant in that particular Chi-squared enrichment test for that dataset and SFARI gene set. The first column indicates the Gencode ID.

Extended Data Figure 3-4. Cort-enriched and TrkB-dependent genes in Harmonizome database. Each Excel tab indicates the enrichment analyses from each disease gene set in the Harmonizome database. For “Bulk” and “IP genotype” tabs, columns represent Harmonizome disease set description, OR (odds ratio of being differentially expressed and in the disease set compared to being differentially expressed and not in the disease set), p.value (p-value from Chi-squared test), adj.P.Val (Benjamini-Hochberg adjusted p-value), setSize (number of genes in the

disease gene set, numSig (number of significantly differentially expressed genes in the gene set), ID (Harmonizome ID), and sigGenes (genes significantly differentially expressed and in the disease set, i.e. those genes driving the enrichment). For “IP vs Input” tab, columns represent Harmonizome disease set description, Enrich_OR (odds ratios from genes significantly more highly expressed in Cort neurons vs. Input), Enrich_Pval (corresponding p-value from Chi-squared test), Deplete_OR (odds ratios from genes significantly more highly expressed in Input vs. Cort neurons), Deplete_Pval (corresponding p-value from Chi-squared test), setSize (number of genes in the disease gene set).

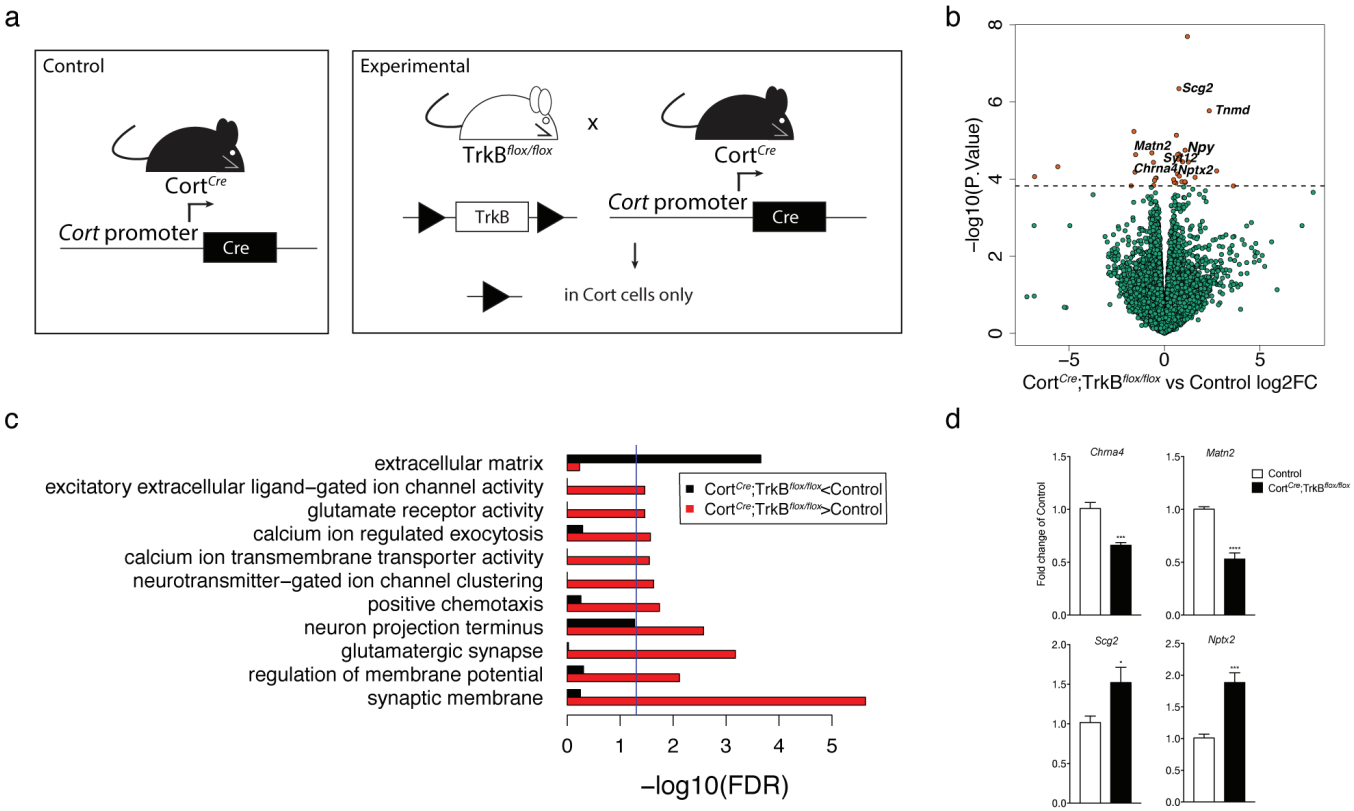

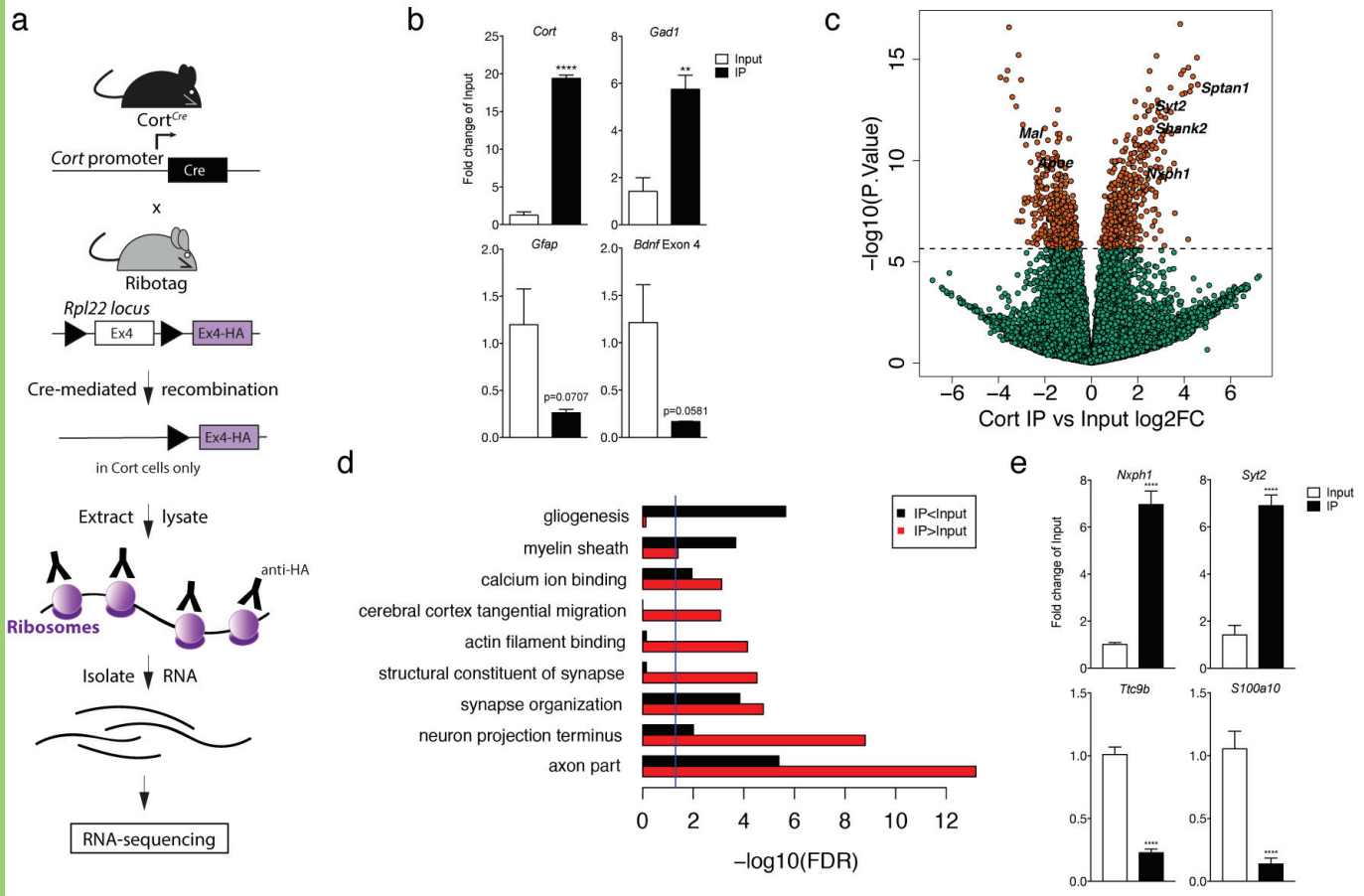

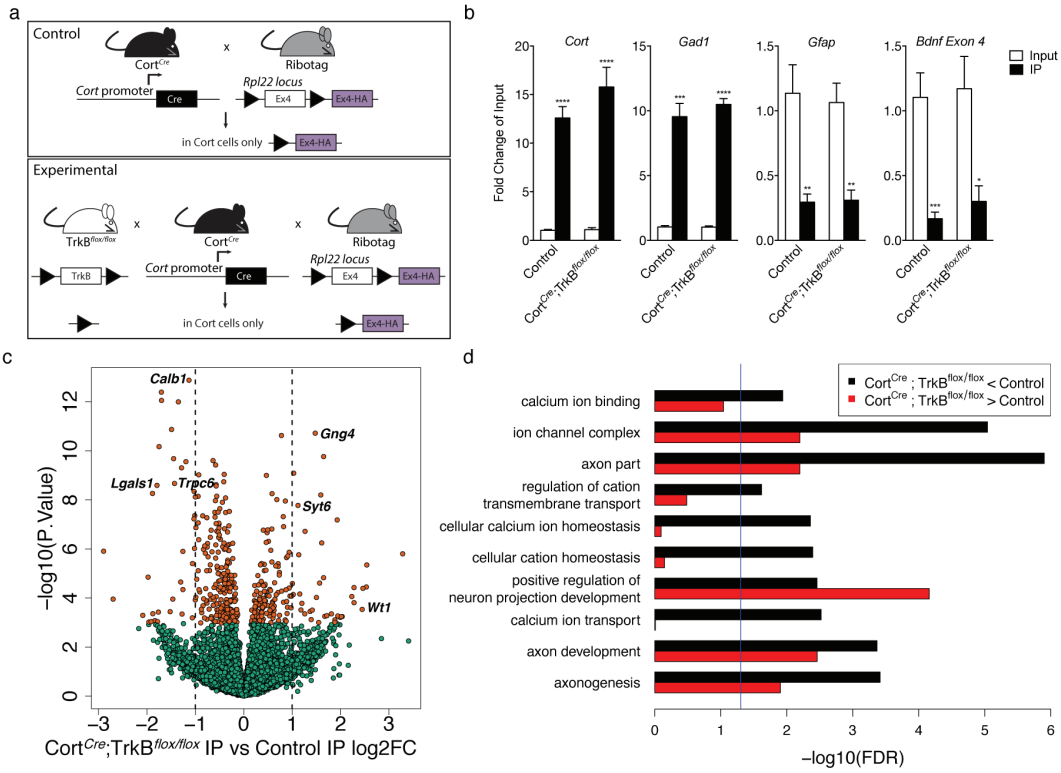

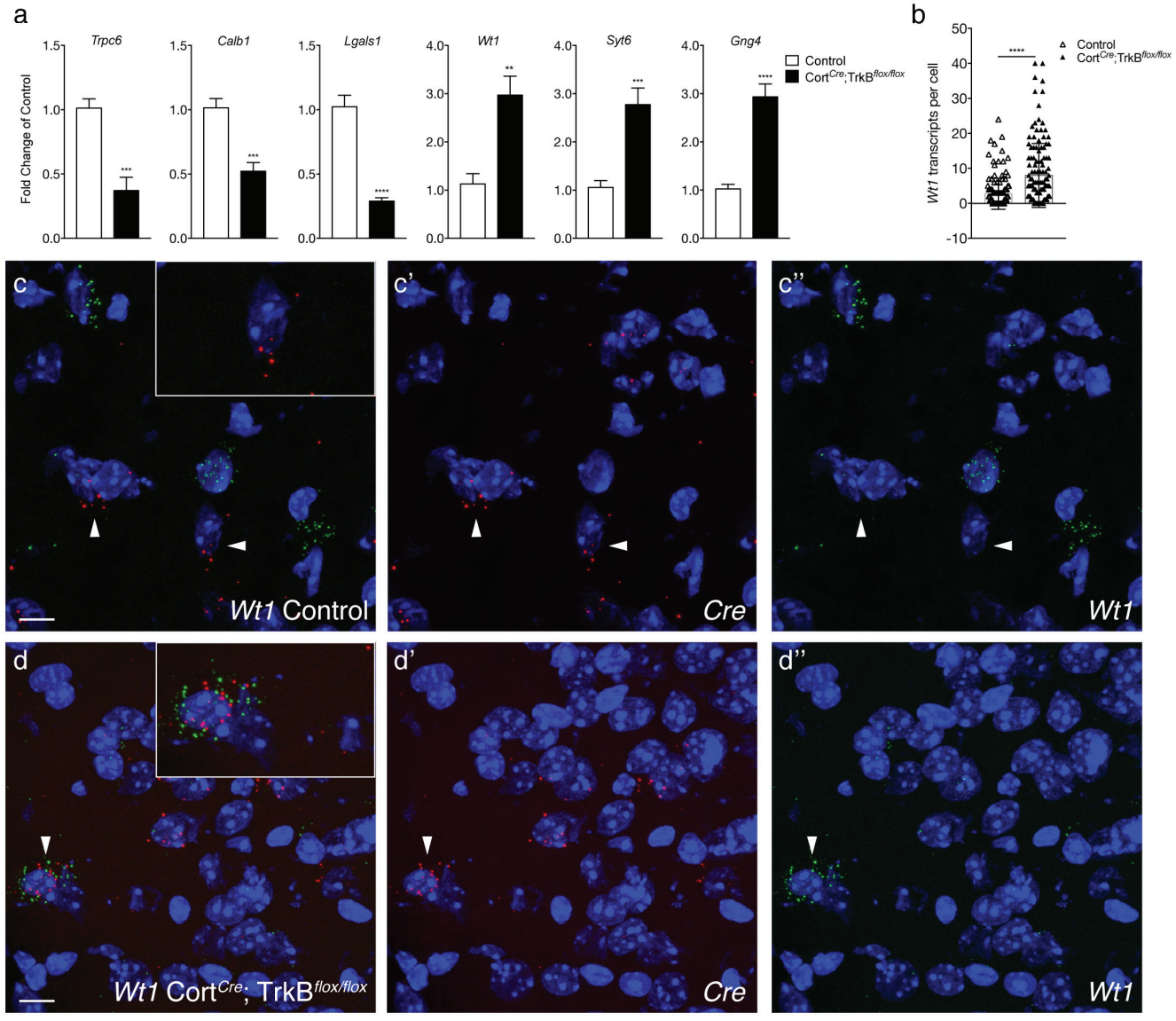

Figure	Data structure	Type of test	Type I error control	Notes
1B	Gene counts for differential expression analysis	Moderated t-tests with linear regression (empirical Bayes)	FDR < 0.1	limma Bioconductor package: voom approach
1C	Gene set enrichment analysis	Hypergeometric test	FDR < 0.05	clusterProfiler Bioconductor package: compareClusters approach
1D	Normalized qPCR data	Student's *t* test	$p < 0.05$	
2B	Normalized qPCR data	Student's *t* test	$p < 0.05$	
2C	Gene counts for differential expression analysis	Moderated t-tests with linear mixed effects modeling (empirical Bayes)	Bonferroni < 0.05	limma Bioconductor package: voom approach
2D	Gene set enrichment analysis	Hypergeometric test	FDR < 0.05	clusterProfiler Bioconductor package: compareClusters approach
2E	Normalized qPCR data	Student's *t* test	$p < 0.05$	
3B	Normalized qPCR data	Student's *t* test	$p < 0.05$	
3C	Differential expression analysis	Moderated t-tests with linear regression (empirical Bayes)	FDR < 0.05	limma Bioconductor package: voom approach
3D	GO enrichment analysis	Hypergeometric test	FDR < 0.05	clusterProfiler Bioconductor package: compareClusters approach
4A	Normalized qPCR data	Student's *t* test	$p < 0.05$	
4B	Normally distributed	Student's *t* test	$p < 0.05$	